Experimental and numerical study of platelets rolling on a von Willebrand factor-coated surface

Justine Pujos, Mathilde Reyssat, Anne Le Goff

Experimental and numerical study of platelets rolling on a von Willebrand factor-coated surface

Justine S. Pujos[a], Mathilde Reyssat[a], Anne Le Goff[a,b,*]

[a] *ESPCI Paris, PSL Research University, CNRS UMR 7083 Gulliver, 10 rue Vauquelin, 75231 Paris Cedex 05, France*

[b] *Sorbonne Universités, Université de Technologie de Compiègne, CNRS UMR 7338 Biomécanique et Bioingénierie, Centre de recherche Royallieu - CS 60 319 - 60 203 Compiègne cedex, France*

Abstract

Blood platelets circulate in the blood and adhere to wounded vessels to initiate coagulation and healing. The first step of this process is the capture of flowing platelets by adhesive molecules located at the wounded vessel wall. In this article, we study the transport of fixed blood platelets in a microfluidic channel coated with von Willebrand factor (vWF), a large multimeric protein expressed by endothelial cells in the vicinity of wounds. We measure the number of platelets adsorbed at the channel surface as a function of both time and space. Experimental results are compared with a new transport model. We show that transverse diffusion is an important feature of our model, while the rolling behavior of the bounded platelets can be neglected.

Keywords: Microfluidics, Platelet, Transport, Rolling, Method of characteristics

List of abbreviations

EFS: Etablissement Français du Sang
PBS: phosphate buffer saline
PDMS: polydimethylsiloxane
PFA: paraformaldehyde
SID: shear-induced diffusion
vWF: von Willebrand factor

Introduction

Platelets are small anucleated blood cells that have an essential role in the process of hemostasis. In a wounded vessel, platelets adhere to the wall through ligand-receptor interactions and initiate coagulation. The large multimeric protein von Willebrand factor (vWF) is such a ligand [1]. At high shear rates, vWF unfolds and exposes platelet-binding domains [2, 3]. The resulting platelet-vWF bonds are transient, causing platelets to roll along a vWF-expressing wall [4, 5].

*Correspondance : anne.le-goff@utc.fr

vWF can also mediate firm adhesion through interaction with activated integrin $\alpha_{IIb}\beta_3$ [6]. Cell rolling is well documented for platelets [7] but also leukocytes [8] and tumour cells [9]. Clinicians need reliable platelet function assays, either for the diagnosis of bleeding disorders [10] or the monitoring of anticoagulant treatments. Microfluidics is a convenient way to manipulate small blood samples [11] and devices have been developed to assess the effects of anti-platelet treatments with measurements of the concentration platelets bound to the surface of a micro-channel [12, 13, 14].

In this article, we study the flow of fixed platelets in a vWF-coated microfluidic chamber. The local concentration of platelets adhering to the wall, C_s, is measured and found to be a decreasing function of the distance x between the channel entrance and the position of observation. This phenomenon, called axial dependency, has been observed in experiments involving whole blood [15]. To the best of our knowledge, although several theoretical and numerical studies focused on the diffusivity of platelets in the transverse direction[16, 17, 18] or on the adhesion mechanism[10], no predictions have been made regarding the axial dependency of platelet concentration.

We present a basic model for the transport of blood platelets in the microchannel. This model involves specific cell-wall interactions and can include advection, diffusion in the transverse direction and cell rolling. The relative importance of the different features of this model is explored through comparison with experimental observations. Physical parameters, such as platelet attachment and detachment rates K_{on} and K_{off}, are used as fitting parameters and we compare their values with experimental measurements or simulated estimations when available.

Experimental Methods

Microfluidics

Microchannels are fabricated using standard soft lithography techniques [19] and have a rectangular cross-section of fixed width $W = 400$ μm and length $L = 4$ cm, and variable height $H \in [14, 63]$ μm. After plasma treatment, channels are sealed on a glass slide, filled with a phosphate buffer saline (PBS, Lonza) solution containing 20 μg.mL^{-1} vWF (Wilfactin, LFB Biomedicaments, Les Ulis, France) and incubated overnight at $4°C$. Prior to the experiment, the channel is rinsed with PBS in order to remove unbound vWF.

The cell reservoir is connected to the channel with capillary tubing (internal diameter 228 μm). The homogeneity of the suspension in the entrance reservoir is maintained by gentle agitation. The flow is driven by a pressure control system (Fluigent MFCS-4C). Platelet perfusions are then performed at a wall shear rate compatible with the unfolding of immobilized vWF ($\dot{\gamma} = 1400 - 1800$ s^{-1}).

Biological Material

Blood platelets isolated from whole blood are provided by Etablissement Français du Sang (EFS) as the following agreement (CPSL C UNT- 06/EFS/029),

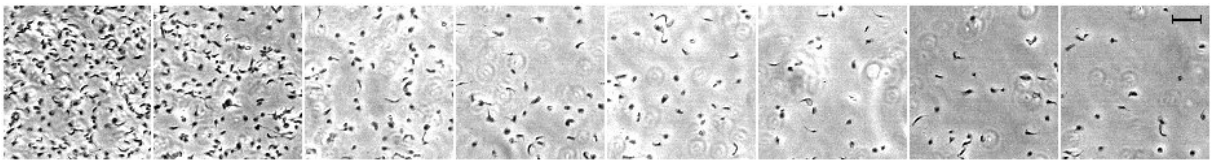

Figure 1: Photographs of the surface of the micro channel after 95 minutes experiment. Positions are equally spaced and separated by 1mm. The first picture is acquired $x = 0.6$ mm away from the channel entrance. Scale bar represents 20 μm.

prepared as described by Dunois-Lardé and co-workers [20], then fixed with paraformaldehyde (PFA), rinsed and diluted in PBS to reach a concentration of 1.4 10^8 mL^{-1}. The goal of fixation is to preserve as much as possible the structure of platelets but to avoid further metabolic reactions, thus preventing effects such as on-chip activation [21].

Videomicroscopy

We use a Leica DMI 6000 B inverted microscope, equipped with a 40x magnification dry lens focused on the glass surface of the chip, and a camera (Photron Fastcam SA3) at an acquisition rate of 0.5 fps with a 20 ms shutter to measure the rolling velocity of adherent cells. During the kinetics measurements, only snapshots are acquired. As the motorized stage navigates between several pre-recorded positions along the whole channel length in less than 2 minutes, the experimental error associated with time is $\Delta t = 1$ min. We define channel entrance, denoted $x = 0$, as the center of the 750 μm-wide hole where inlet tubing is inserted. The precision for position is therefore of the order of 300 μm. Images are analysed with ImageJ software, using a routine to automatically count the number of adherent cells in a microscope field. In the case of dense surface coverage, the program fails to separate entangled platelets. Such images are analysed independently by two experimentalists. The discrepancy between their two counts was used to estimate the measurement error on platelet surface concentration $\Delta C_s \sim 20\% C_s$.

Experimental observations

Figure 1 shows photographs of the channel surface after 95 minutes of perfusion, showing evidence of the axial dependency of platelet adsorption. The exposure time is long, so that only platelets bound to vWF appear sharp. Flowing platelets are not visible.

Figure 2 illustrates the diversity of behaviours observed at the surface. Positions of surface-adsorbed platelets are shown, with time colour-coded from purple to red. Some platelets roll along the surface, creating rainbow-like patterns, while others are stationary and appear white. Events of platelet adhesion and desorption from the surface also occur, generating incomplete rainbows.

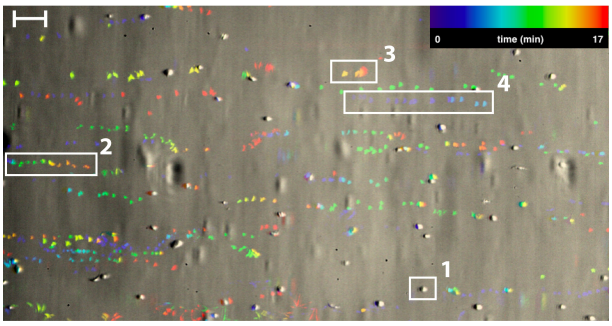

Figure 2: Superposition of pictures from a video focused on the surface of the micro-channel. The colors from blue to red corresponds to the time, the scale is 20μm. Both stationary platelets (frame 1) and rolling platelets (frame 2) can thus be observed. One adhesion event is identified in (frame 3) as the first time this platelet is measured is in the middle of the experiment. Likewise a desorption event is seen (frame 4) as the platelet disappears from the surface before the end of the experiment.

Model

Based on the above observations, we develop a model which describes the transport of blood platelets in the channel. Our goal is here to understand the physical phenomena governing the repartition of platelets between volume and surface along the channel. Three types of dynamical events are involved in the model: adhesion, desorption and rolling.

Equations

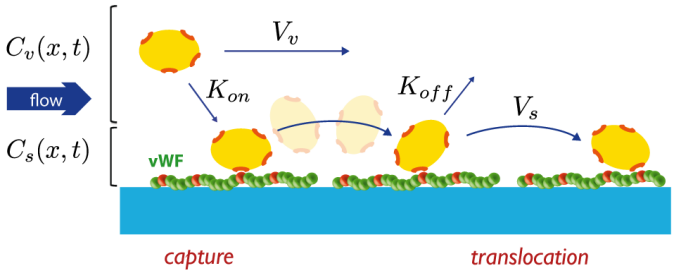

Figure 3: Interactions of platelets with the vWF-coated wall. Platelets in the volume are advected with a speed V_v and can bind with the vWF with a coefficient K_{on}. Adherent platelets can roll with a speed V_s and detach with a coefficient K_{off}.

As shown in Figure 3, we define a small control volume and consider the number of platelets in this volume and on the surface, respectively noted n_v

and n_s. The mass balance sketched in Figure 4 involves their time variations:

$$\begin{cases} n_v(x, t+dt) \\ \quad = n_v(x,t) \ + \ n_{v,in} \ - \ n_{v,out} \ - \ n_{exch} + \ n_{diffusion} \\ n_s(x, t+dt) \\ \quad = n_s(x,t) \ + \ n_{s,in} \ - \ n_{s,out} \ + \ n_{exch} \end{cases} \tag{1}$$

where $n_{v,in}$ and $n_{v,out}$ (resp. $n_{s,in}$ and $n_{s,out}$) are the number of cells that enter and exit the volume (resp. surface) due to advection (resp. rolling) during dt. n_{exch} represents the number of cells exchanged between surface and volume. The additional source term $n_{diffusion}$ will be discussed later.

The exchange term n_{exch} is composed of two parts. The formation of bonds between vWF and platelets on the one hand is described by the adhesion rate K_{on}, depending linearly on the number n_v of available platelets, and limited by the presence of platelets already on the surface. On the other hand, for the detachment of platelets, with a rate K_{off}, from the surface, only a linear dependency with the number of adsorbed platelets is considered, as platelet suspensions are dilute enough in our experiments:

$$n_{exch} \ = \ K_{on} \ dt \ n_v \ (1 - n_s/n_{s,max}) - K_{off} \ dt \ n_s$$

with $n_{s,max}$ the maximum number of platelets that can adhere to the control surface.

We rewrite equation (1) using the volume and surface concentration of platelets:

$$\begin{aligned} n_{v,in} &= C_v(x,t) \ V_v \ dt \ h \ dy \\ n_{v,out} &= C_v(x+dx,t) \ V_v \ dt \ h \ dy \\ n_{s,in} &= C_s(x,t) \ V_s \ dt \ dy \\ n_{s,out} &= C_s(x+dx,t) \ V_s \ dt \ dy \end{aligned} \tag{2}$$

Here, h represents the thickness of the fluid layer interacting with the surface. In an extremely shallow channel, all platelets in the bulk interact with the walls and the concentration C_v in the exchange layer is equal to the average bulk concentration in the channel. In some situations however, the influence of the wall may not reach the core of the flow. The region involved in the exchanges with the wall is more shallow than the channel. There, new platelet adhesion events can induce a significant decrease of the volume concentration C_v. This depletion can be compensated by a diffusive term. Calling D the diffusion coefficient, n_v^∞ the quantity of platelets in the bulk, above the exchange layer, and l_D the typical distance over which diffusion occurs, we get: $n_{diffusion} = D \ dt \ / l_D^2 \ (n_v^\infty - n_v)$.

Introducing the partial derivatives of the concentration with respect to time

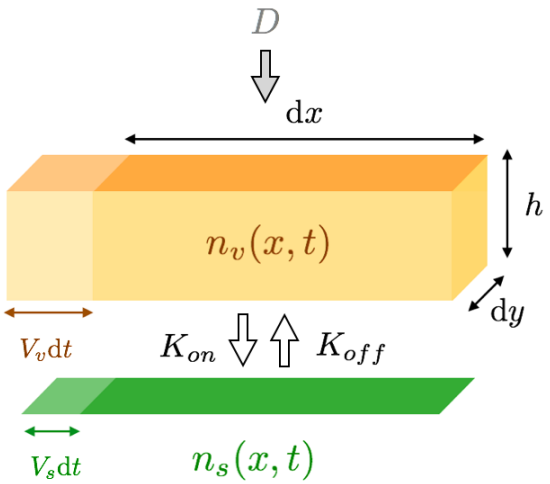

Figure 4: The wall surface in green and the volume in orange respectively contain $n_s(x,t)$and $n_v(x,t)$ platelets at the time t in the space between x and $x+dx$. The platelets in the lighter region enter these spaces between t and $t+dt$.

and space, we get:

$$\begin{cases} \dfrac{\partial C_v}{\partial t} + V_v \dfrac{\partial C_v}{\partial x} &= -J \ + \ \dfrac{D}{l_D^2} \ (C_v^\infty - C_v) \\ \dfrac{\partial C_s}{\partial t} + V_s \dfrac{\partial C_s}{\partial x} &= hJ \\ J = K_{on} C_v \left(1 - \dfrac{C_s}{C_{s,max}}\right) &- \ K_{off} \dfrac{C_s}{h} \end{cases} \tag{3}$$

C_s, C_v and C_v^∞ are respectively the surface concentration, the volume concentration in the exchange layer and the volume concentration in the bulk; $C_{s,max}$ the maximal concentration on the surface at the packing limit.

Initially, both the surface and the volume of the channel are empty:

$$\begin{cases} C_v(x, t=0) \ = \ 0 \\ C_s(x, t=0) \ = \ 0 \end{cases} \tag{4}$$

At the channel entrance, new platelets are injected in the volume only:

$$\begin{cases} C_v(x=0, t) \ = \ C_v^\infty \\ C_s(x=0, t) \ = \ 0 \end{cases} \tag{5}$$

Dimensionless equations

From equation (3), we can apply a series of basic transformations described in the Appendix A to reach the following dimensionless equations:

$$\begin{cases} v_t + v_x \ = -j + d(v^\infty - v) \\ s_t + \epsilon s_x \ = j \\ j = v\ (1 - s)\ -\ \alpha s \end{cases} \tag{6}$$

and boundary conditions:

$$\begin{cases} v(x, t = 0) \ = 0 \\ s(x, t = 0) \ = 0 \\ v(x = 0, t) \ = v^\infty \\ s(x = 0, t) \ = 0 \end{cases} \tag{7}$$

where v, s and v^∞ are the dimensionless concentrations C_v, C_s and C_v^∞ respectively, and the subscripts represent partial derivation with respect to dimensionless time and space. The parameters d, ϵ and α are defined as a non-dimensional diffusion coefficient $d = \frac{D}{l_D^2 K_{on}}$, the ratio of longitudinal velocities $\epsilon = \frac{V_s}{V_v}$ and the ratio of exchange rates $\alpha = \frac{K_{off}}{K_{on}}$.

Here the system is composed of two half-spaces v and s, where a same object has different speed 1 and ϵ and an exchange value j between the half-spaces. The diffusion can be easily added or neglected. These dimensionless coupled equations thus offer the opportunity to generalise this study to any similar system.

Analytical approach

The equations (6) represent the transport of a population in two interacting spaces with different characteristic speeds. We apply here the method of characteristics to these coupled equations. Briefly, three subspaces are defined in the (t, x) plane, as shown in Figure 5: a yellow domain where $x > t$, a grey domain where $\epsilon t < x < t$ and a blue domain where $x < \epsilon t$. The boundaries of these subspaces are lines of constant speed, as 1 and ϵ are the non-dimensional speeds of the cells in the volume and at the surface respectively. We can define two sets of characteristic curves in the (t, x) space, one for each concentration v and s. The set of curves $\mathcal{K}_1$ is defined by $\frac{dx}{dt} = 1$ (blue lines in Figure 5) and the equation $\frac{dv}{dt} = -j(s, v) + d(v^\infty - v)$ is true on them; the set of curves $\mathcal{K}_\epsilon$ is defined by $\frac{dx}{dt} = \epsilon$ (red lines in Figure 5) and associated with $\frac{ds}{dt} = j(s, v)$.

Let us consider the blue sub-space defined by $x < \epsilon t$ and the point $M_1(t_1, x_1)$ as shown in Figure 6. Since the evolution of v is known on the characteristic lines of slope 1 and that of s on lines of slope ϵ, the values v_1 and s_1 at M_1 only depend on the initial values of v and s at M_0 and M_0' and on the distance on each characteristic, that is to say on x_1.

If $\tilde{M_1}$ is also in the sub-space and at the same height x_1 as M_1, then the solutions v and s are identical to those of M_1, since they derive from the values

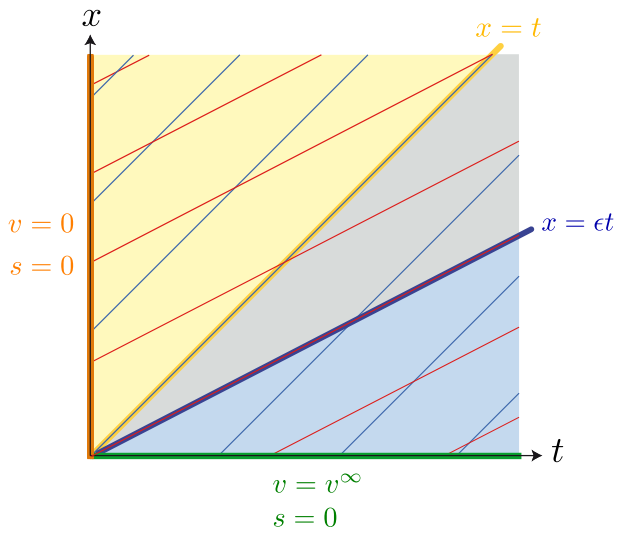

Figure 5: Characteristic curves defined from the coupled equations (6) in the (t, x) space. Three sub-spaces are presented here: in yellow the sub-space defined by $x > t$, in blue the sub-space $x < \epsilon t$ and grey the sub-space between the two and where most of the interesting physics of the system resides.

measured in $\tilde{M}_0$ and $\tilde{M}'_0$, that are the same as in M_0 and M'_0. Thus all points at a position (t, x_1) with $t > x_1/\epsilon$ share similar values of the concentrations s and v since they originate from a similar boundary condition $v = v^{\infty}$ and $s = 0$. This means that, for each position x, the system reaches a stationary state for $t > x/\epsilon$. Experimentally, this fact is confirmed for small positions. For large positions, no stationary state is observed, because the condition $t > x/\epsilon$ is not achieved during the course of the experiment.

A similar approach shows that the sub-space defined by $t < x$ has solutions that do not vary with position. If diffusion is neglected ($d = 0$), then the concentrations in this subspace are zero, as no object can move faster than the highest speed in the system and the only source of platelets is the injection at the origin of the channel ($v(t, x = 0) = v^{\infty}$). When diffusion is considered, it is the only source of cells in this subspace. The solution still does not change with respect to the position, because the diffusion coefficient is a constant and the boundary conditions are the same all along the channel.

Figure 7 shows how, having explored these asymptotic regimes, we can sketch the shape of kinetics and axial dependency curves. The region explored in experiments corresponds to the grey zone and not to the asymptotic regimes described above. The temporal resolution of our experiments does not allow us to capture the delay between starting times at different positions. For example, for two positions x_1 and x_2, we expect kinetics curves to start with a delay $\tau = \frac{x_2 - x_1}{V_v}$. If V_v is 1 mm·s^{-1}, which is the order of magnitude of the average bulk velocity, then even for the largest possible separation $x_2 - x_1 = 4$ cm, we

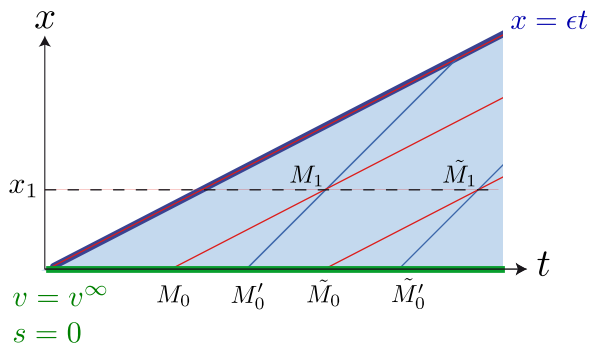

Figure 6: Details of the sub-space defined by $x < \epsilon t$ where M_0 and M_0' (respectively $\tilde{M}_0$ and $\tilde{M}_0'$) are the boundary conditions relative to M_1 (respectively $\tilde{M}_1$). On the horizontal axis, values of v and s are fixed to v^∞ and 0. From these values, the solution at the point $M_1(t_1, x_1)$ can be calculated. This solution is similar to the one at the point $\tilde{M}_1(\tilde{t_1}, x_1)$ as they originate from the same set of equations and previous states. Thus, all points on the line $x = x_1$ at times larger than x_1/ϵ share the same values of v and s, and the solution is stationary in this subspace.

find $\tau < 1$ min. In spite of this, the overall shape of kinetics curves resembles that of experimental ones.

Numerical resolution

In order to explore the intermediate zone, we use a time-step numerical method to solve equation 6. We compute volume and surface platelet concentrations for all values of x and t, and not only in asymptotic cases. The programs are written in *Matlab* and run on a recent Intel-based desktop computer.

The equations involve seven parameters. d, ϵ and α describe the physics of the system, while the other four render time t, position x and the two concentrations C_v and C_s dimensionless. We look for the set of parameters which yields the simulation closest to the experimental points. We can thus describe this as minimizing a score function in a seven-dimensional space. The score value r is a simple distance between simulated and experimental points. Since the parameters do not appear explicitly in the score function, we can not run a classical optimisation search. Indeed, a whole simulation must be re-run for each set tested. We thus wrote a simplified search process, sketched in Figure 8.

We start the search with a limited number of different values for each parameters and test all possible combinations. All parameters are varied on a logarithmic scale with the exception of $C_{s,max}$ which is tested on a linear scale. We then select the two sets which lead to the best fits between simulation and experiments but differ by more than one parameter. All combinations are tested for the two previously selected sets. At each iteration, we keep the two best fits and use them as input for the next refinement. Every three iterations, the dif-

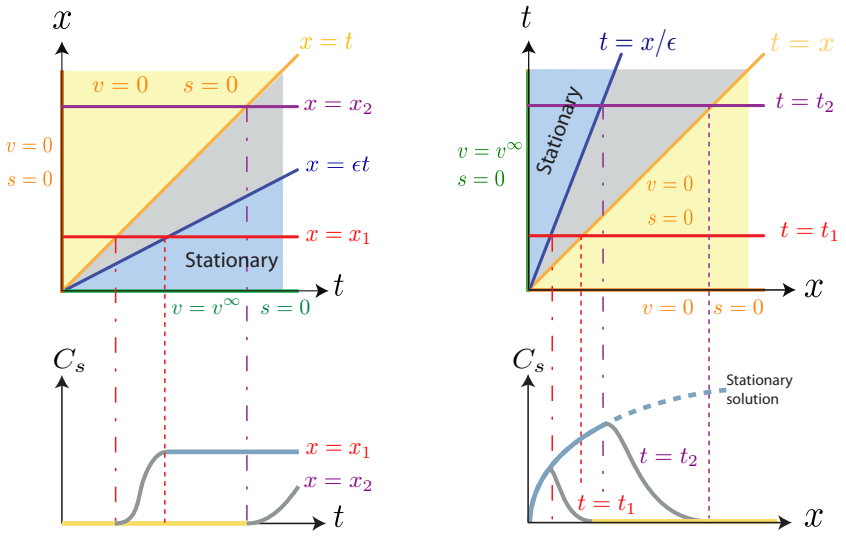

Figure 7: A kinetics (resp. axial dependency) curve is built by intersecting a horizontal line with the (t, x) (resp. (x, t)) diagram. Significant variations occur when this line cross the grey region, connecting with the two asymptotic solutions at times (reap. positions) defined by the dashed lines.

ference between the input values and the tested parameters is reduced so we can reach a greater precision for the result.

The selection of the two best fits aims to avoid finding a local minimum of our score function instead of the global minimum we are looking for. This search pattern, and in particular the fact that we limit our search to nine iterations, determines the maximum values each parameters can reach. An a-posteriori verification is performed: the values found at the end of the search should not be at the border of the search range.

	$C_{s,max}$ (mm^{-2})	V_v ($\mathrm{mm{\cdot}s}^{-1}$)	V_s ($\mathrm{mm{\cdot}s}^{-1}$)	K_{on} (s^{-1})	K_{off} (s^{-1})	D ($\mathrm{mm}^2{\cdot}\mathrm{s}^{-1}$)	h (mm)
min	$5\ 10^3$	$1.7\ 10^{-5}$	0	$1.7\ 10^{-6}$	10^{-12}	0	10^{-7}
max	$13.6\ 10^4$	373	373	37.3	37.3	10^2	1

Table 1: Extreme values used in the search process.

Discussion

We start by using a simplified model without diffusion. Table 1 contains the range of variation for all the other parameters. Figure 9 shows that the model provides an overall shape consistent with experimental measurements, consisting of an initial increase followed by saturation, close to the channel entrance. The

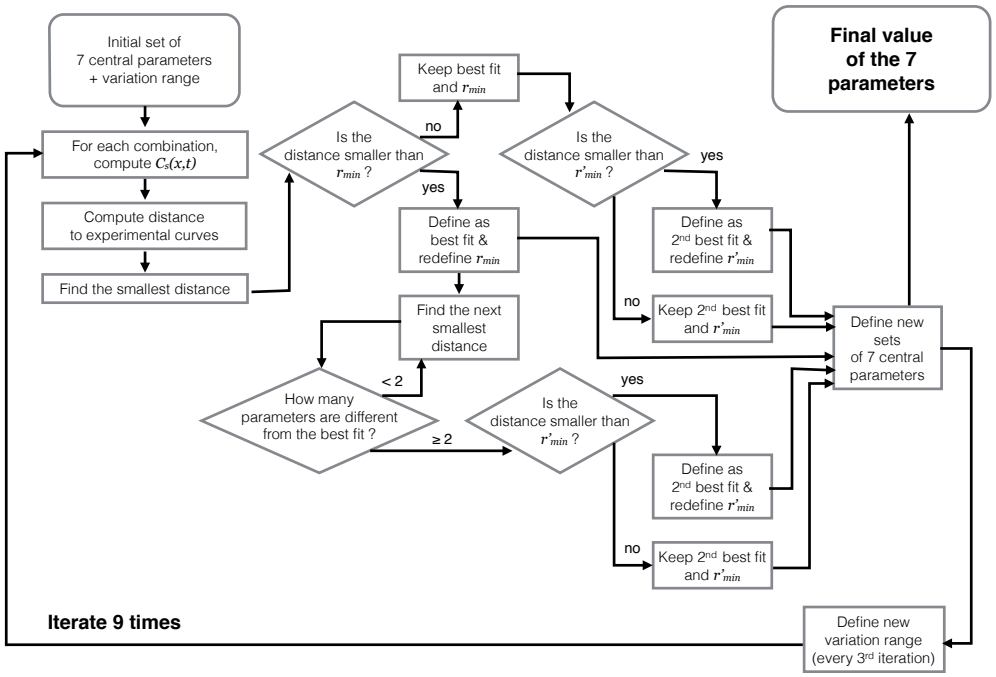

Figure 8: Flow chart representing the fitting process.

saturation is no longer observed further away from the entrance ($x > 4$ mm). For distant positions, experimental curves are concave while numerical ones are convex. Before trying to refine the model to better adjust the shape of experimental curves, let us discuss the order of magnitude obtained for the model parameters, presented in Table 2.

$C_{s,max}$ is defined as the threshold beyond which no new platelets can adsorb to the surface. This situation may occur when all the vWF binding sites are used, or if the platelet close packing limit is reached. As the surface is densely coated in vWF, we expect the second situation to be the limiting factor. Considering platelets as discs of average diameter 3.1 μm [22], the maximal 2D packing fraction is reached when $C_{s,max} \simeq 12 \cdot 10^4$ mm^{-2}. The value found with our algorithm $1.7 \cdot 10^4$ mm^{-2} is smaller than this estimation. This can be easily explained, as many platelets in our sample have a shape more complex than a discoid, and the packing of such objects cannot be as compact as that of discs. Also, in the vicinity of adherent platelets, perturbations of the local flow may prevent new platelets from being captured by the surface.

The adsorption rate of the model is taken as $K_{on} = 0.24$ s^{-1}. This value is

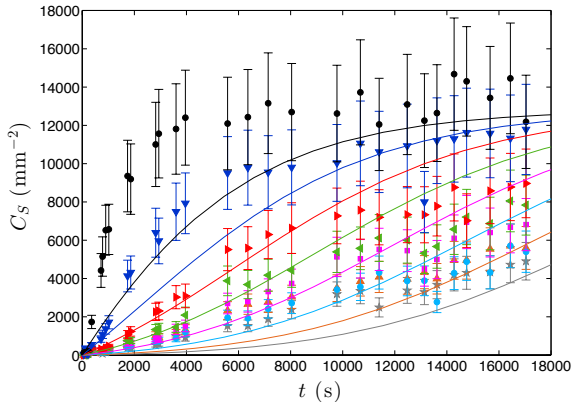

Figure 9: Temporal evolution of the surface concentration of platelets at different positions in the channel: $x = 0.6$ mm (●) $x = 1.6$ mm (▼), $x = 2.6$ mm (▶), $x = 3.6$ mm (◀), $x = 4.6$ mm (■), $x = 5.6$ mm (●), $x = 6.6$ mm (▲), $x = 7.6$ mm ($\star$). Solid lines represent numerical predictions obtained by neglecting diffusion.

consistent with the rate constant associated with the transition of free platelets from the volume to a surface bounded state, that was estimated by Fitzgibbon et al. [23]: $r_{2-3} \simeq 0.07 - 0.4$ s^{-1}. When modeling the adhesion of platelets to subendothelial matrix, Leiderman and Fogelson [24] find a value of 1 s^{-1}. In this situation, platelet adhesion is mediated by a larger number of molecules than vWF alone, which can explain this larger adhesion rate.

The desorption rate K_{off} is found to be much smaller than K_{on}: $K_{off} \simeq 6\ 10^{-5}$ s^{-1}. This small value is due to the dense coating of vWF which forms several bonds with each platelet, that have to be simultaneously broken for the platelet to be released. Experimental measurements with platelet-rich plasma on a non-adhesive surface yield a value $k_{off} \simeq 5 \cdot 10^{-2}$ s^{-1} [25]. It is reasonable that the value we measure on an adhesive surface much smaller.

The length h is the height in the volume where platelets can interact with the surface and form bonds. We find $h \simeq 0.1$ μm which is in agreement with the size used by Fitzgibbon et al. [23]: $L = 0.2$ μm. This also corresponds to the diameter of the repeating units constituting the vWF protein [2]. Because h is smaller than the size of a single platelet, the volume concentration in the layer of thickness h should rather be considered as a probability for a platelet from the bulk to reach the surface and adhere to it.

The advection velocity V_v is found to be 0.36 mm $\cdot$ s^{-1}. The average fluid velocity in the channel is much larger $\bar{V} \sim 6$ mm$\cdot$s^{-1}. But in the exchange layer located close to the channel bottom the velocity can be estimated as $V_v = \dot{\gamma} h/2$. This yields a prediction for $V_v \sim 0.6$ mms $\cdot$ s^{-1}, that is in fair agreement with the value provided by the fit.

The rolling velocity V_s is the only parameter whose fitted value seems inconsistent. The typical velocity of rolling platelets is 1 to 10 μm$\cdot$s^{-1}, which is 5

orders of magnitude beyond the numerical result. The decrease in average velocity could be explained by the presence of platelets activated prior to fixation and incapable of rolling. This is consistent with experimental observations of a few immobile platelets.

Influence of diffusion

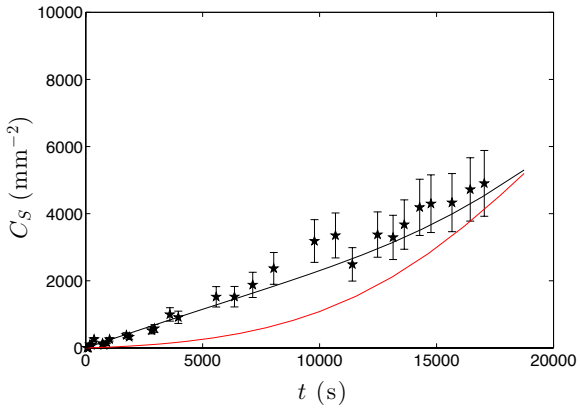

Figure 10: Adsorption kinetics 7.6 mm away from the channel entrance. Experimental data are compared with numerical simulations obtained with a simple model neglecting (in red) or taking into account diffusion (in black).

Far from the entrance, our model fails to capture the curvature of kinetics curves. This underestimation of platelet adsorption suggests that a source term is missing from the initial model. A possible explanation is that platelets diffuse from the core of the channel towards the walls. Brownian diffusion is parametrized by the coefficient $D_B = k_B T/(6\pi\eta R) \sim 2\ 10^{-13}$ m^{2}s^{-1}, with the water viscosity $\eta_{water} \sim 10^{-3}$ Pa $\cdot$ s and the particle radius $R \sim 10^{-6}$ m. Shear-induced diffusion (SID) is defined as an effective diffusive motion of particles in a shear flow. It increases with shear rate and depends on the shape of diffusing objects [26]. The SID coefficient is written $D_{SID} = \dot{\gamma} R^2 f(\phi)$, with $\dot{\gamma} = 1400$ s^{-1} the local shear rate, and $\phi \sim 0.5\ 10^{-3}$ the volume fraction of the particles. For anisotropic particles, the function f is different than for spherical particles and the diffusivity is more important [18]. In the dilute limit the diffusivity is proportional to ϕ and we can estimate the diffusion coefficient for plate-like objects [26]: $D_{SID} = \dot{\gamma} R^2\ 6.9\ \phi \sim 6.2\ 10^{-12}$ m^{2}s^{-1}. It thus appears that shear-induced diffusion should predominate over Brownian diffusion in our system.

The Peclet number $Pe = \frac{\tau_{diff}}{\tau_{conv}}$ compares diffusion and convection time scales. Here, $Pe = \frac{V_v l_D^2}{DL}$, with l_D the typical distance over which diffusion occurs in the transverse direction and $L \sim 10^{-3}$ m the distance between two

measurements. Here we consider that l_D is of the order of the channel thickness $H \sim 10^{-5}$ m [27]. We get $Pe \sim 2$, indicating that diffusion cannot be neglected.

When diffusion is taken into account, numerical curves lose their convexity, as illustrated in Figure 10. The best fit is obtained for $D = 5.9\ 10^{-12}\ \mathrm{m^2 s^{-1}}$, which is in fair agreement with theoretical predictions. The value of parameters obtained with this full model, presented in the second line of Table 2, remain consistent with the estimations presented in the previous paragraph.

Influence of the rolling behaviour

Even when diffusion is taken into account, the value of V_s deduced from the model remains extremely low. In the equation expressing transport at the surface, the term $V_s \frac{\partial C_s}{\partial x} \sim V_s \frac{C_{s,max}}{L}$ can balance the desorption term $K_{off} C_s$ if $V_s \sim K_{off} L$, that is of the order of 0.1 $\mu\mathrm{m{\cdot}s^{-1}}$. The adjusted values of V_s are several orders of magnitude smaller. This seems to indicate that rolling can be neglected in our problem. In supplementary Figure 12, we adjust experimental data with new numerical simulations in which rolling velocity is set to 0. Of course, in a different system where the velocity contrast between surface and volume is smaller, we could expect a significant contribution from rolling to surface coverage. Again, the values of all parameters stay in the same order of magnitude, although they may vary by a factor 2 or 3. Thus the rolling behaviour of platelets seems negligible in this case. Nevertheless, it may very well be fundamental for the formation of blood clots, such as in microfluidic models of stenosis and coagulation [12, 28].

Influence of the non-linearity

Experimental values of C_s never exceed 15000 $\mathrm{mm^{-2}}$, a much smaller value than those obtained for $C_{s,max}$ in the best fits. We further simplify the model by suppressing the non-linear surface saturation term:

$$1 - \frac{C_s}{C_{s,max}} \simeq 1$$

in equation (3). Far from the channel entrance, the linear model yields results that are very similar to the ones obtained with the full model. As seen in supplementary Figure 13, results are less satisfying close to the channel entrance, where the surface coverage is maximal. As suppressing the non-linear term represents a significant gain of time, this linear model could be interesting for applications where a prediction of surface coverage far from the channel entrance is desired.

Influence of desorption

Since the desorption rate K_{off} is much smaller than that of the adsorption rate K_{on}, we also attempt to adjust experimental curves while neglecting desorption. The results are displayed in Figure 11: the obtained numerical curves increase fast and clearly fail to grasp the trend towards saturation exhibited by experimental data. In fact, although both rates share the same dimension,

	$C_{s,max}$ (mm^{-2})	V_v ($\mathrm{mm\cdot\ s}^{-1}$)	V_s ($\mathrm{mm\cdot\ s}^{-1}$)	K_{on} (s^{-1})	K_{off} (s^{-1})	D ($\mathrm{mm}^2\mathrm{s}^{-1}$)	h (mm)
no diffusion	$1.7 \cdot 10^4$	0.36	$3.6 \cdot 10^{-11}$	0.24	$0.6 \cdot 10^{-4}$	0	$0.9 \cdot 10^{-4}$
full	$3.8 \cdot 10^4$	0.10	$1.0 \cdot 10^{-10}$	0.18	$3.6 \cdot 10^{-4}$	$5.9 \cdot 10^{-6}$	$2.7 \cdot 10^{-4}$
no rolling	$6.1 \cdot 10^4$	0.04	0	0.05	$3.4 \cdot 10^{-4}$	$1.7 \cdot 10^{-6}$	$7.8 \cdot 10^{-4}$
linear	$5.4 \cdot 10^4$	0.03	$3 \cdot 10^{-13}$	0.04	$3.2 \cdot 10^{-4}$	$1.7 \cdot 10^{-6}$	$9.3 \cdot 10^{-4}$
no desorption	$1.2 \cdot 10^5$	0.01	0	0.03	0	$0.7 \cdot 10^{-6}$	$2.7 \cdot 10^{-3}$
literature	$1.2 \cdot 10^5$			0.07 - 1	0.05	$6.2 \cdot 10^{-6}$	$2 \cdot 10^{-4}$
reference	[22]			[23, 24]	[25]	[26]	[2, 23]

Table 2: Parameters value for the different models tested

they should not be directly compared with one another. The exchange rate J involves two terms, $K_{on}C_v$ and $K_{off}\frac{C_s}{h}$ that are actually of the same order of magnitude when computed with the fitting parameters. It is thus necessary to keep the desorption term in the analysis.

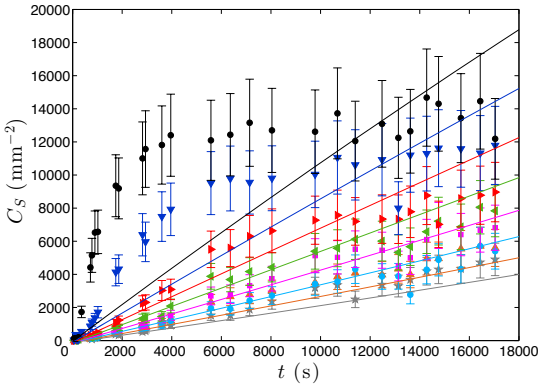

Figure 11: Temporal evolution of platelet surface concentration at different positions in the channel: $x = 0.6$ mm (●) $x = 1.6$ mm (▼), $x = 2.6$ mm (▶), $x = 3.6$ mm (◀), $x = 4.6$ mm (■), $x = 5.6$ mm (●), $x = 6.6$ mm (▲), $x = 7.6$ mm (⋆). The experimental points with their error bar are compared with the model obtained when no desorption is considered (lines).

Variability

The weak contribution of rolling to the transport of platelets along the channel may be explained by the fact that some of the adherent platelets are activated and do not translocate. This feature is likely to vary from one sample to another. In supplementary Figure 14, we show that the shape of adhesion kinetics changes when experimental conditions are varied, but the main features, such as axial dependency and saturation close to the entrance, are conserved. Parameters such as channel height, platelet sample, platelet concentration and wall shear rate are varied (see supplementary Table 3). While the model without

rolling remains in fair agreement with experimental data for other samples, the adjusted diffusion coefficient can be as much as three orders of magnitude lower than the one measured for sample A. In shear-induced diffusion, the apparent diffusion coefficient strongly depends on the particules' size and aspect ratio. Platelets have a roughly discoidal shape, but for some patients, blood also contains incompletely formed, larger platelets that have a dumbbell shape. It can therefore be understood that shear-induced diffusion plays a significant role in platelet transport for some, but not all patients.

We also notice that the adjusted value of K_{on} is small for this particular sample (sample B). This is consistent with the measured values of platelet concentration that remain low even at long times, indicating that the affinity of platelets from this sample for vWF is smaller than usual.

For yet another example (sample C), the shape of kinetics curves and results of fitting are more similar to the ones obtained with sample A, as well as the values of the fitting parameters. The shape of curves at intermediate positions however is not well reproduced by the simulations. The axial dependency is very marked in this experiment, and the values of C_s measured at positions far from the entrance are almost uniformly equal to 0. These data with extremely low values bias the fitting process, that becomes therefore less efficient in the regions of finite C_s. The choice of the observation positions for this experiment is not optimal. A more accurate fitting could be performed by selecting only the experimental data containing significant information.

Conclusions

We presented in this article an experimental set-up and an associated model to study the transport of fixed blood platelets in a micro channel with coated walls. In spite of the variations that we observe between models or between experiments, some of the conclusions are repeatable. In all three examples, we find that the thickness of the exchange layer h is of the order of a few hundred nanometers. The adsorption and desorption constants K_{on} and K_{off} extracted from this work characterize the behavior of whole cells and not of single bonds. The desorption rate K_{off} is always much smaller than K_{on} but desorption is not negligible and accounts for the saturation observed close to the channel entrance. In some samples, shear-induced diffusion needs to be taken into account and the diffusion coefficient D found by adjusting experimental data is in agreement with theoretical predictions. To further improve the fitting, we would need to take into account the fact that diffusion occurs across the cell-free layer, whose thickness is not uniform. By choosing a constant characteristic length for diffusion, we underestimated the diffusive flux towards the surface close to the channel entrance, where the cell-free layer is extremely thin and the concentration gradient large.

When whole blood is used instead of a platelet suspension, the surface is covered much more rapidly [15]. This is due to margination effects : red blood cells present in the core of the vessel flow push platelets towards the surface, increasing their availability in the vicinity of the walls [17]. We assume that our

model could remain valid in such a situation, if an effective diffusion coefficient depending on red blood cell concentration and deformation replaced the shear-induced diffusion coefficient.

We also quantified axial dependency and showed that concentration profiles exhibit extremely sharp decreases close to the channel entrance. Measurements of the surface concentration in adsorbed platelets is therefore highly sensitive to a small error in position. We therefore think that experiments where observations are made on a single location in the channel should be handled with care, and that measurements made at several positions should be preferred.

Although sophisticated multiscale models exist, practical applications could make use of less costly micro scale simulations [29]. This paves the way towards more efficient simulations of cell suspension dynamics.

Acknowledgements

Work financed in part by ANR RPIB 2011-009 grant and Fondation Pierre-Gilles de Gennes. We wish to thank Dominique Baruch and Aurélie Magniez who prepared the platelets; Antoine Blin and Hyacinthe Buisson who performed preliminary experiments; and Olivier Dauchot for inspiring discussions.

Appendix A: Dimensionless equations

The goal is to render the following coupled equations dimensionless:

$$\begin{cases} \dfrac{\partial C_v}{\partial t} + V_v \dfrac{\partial C_v}{\partial x} &= -J \ + \ \dfrac{D}{l_D^2} \ (C_v^\infty - C_v) \\ \dfrac{\partial C_s}{\partial t} + V_s \dfrac{\partial C_s}{\partial x} &= hJ \\ J = K_{on} C_v \left(1 - \dfrac{C_s}{C_{s,max}}\right) \ - \ K_{off} \dfrac{C_s}{h} \end{cases}$$

We first focus on the two concentrations and apply the following transformation:

$$C_v \ \longleftarrow \ \frac{C_v \, h}{C_{s,max}} = v$$
$$C_s \ \longleftarrow \ \frac{C_s}{C_{s,max}} = s$$

The transversal dimension h is naturally used to bridge the gap between the surface and volume concentrations as it is characteristic of the dimension that differ between the two concentrations. The equations thus transform into:

$$\begin{cases} \dfrac{\partial v}{\partial t} \ + V_v \dfrac{\partial v}{\partial x} &= -\tilde{J} \ + \ \dfrac{D}{l_D^2} \ (v^\infty - v) \\ \dfrac{\partial s}{\partial t} \ + V_s \dfrac{\partial s}{\partial x} &= \tilde{J} \\ \tilde{J} \ = \dfrac{Jh}{C_{s,max}} = K_{on} v \, (1 - s) \ - \ K_{off} \ s \end{cases}$$

We then render time and position dimensionless using the characteristic speed V_s and characteristic time $1/K_{on}$.

$$\begin{aligned} t &\longleftarrow t\, K_{on} \\ x &\longleftarrow x\, K_{on} \,/\, V_v \end{aligned}$$

which leads to the following coupled equations:

$$\begin{cases} v_t \;+\; v_x \;= -j \;+\; \dfrac{D}{l_D^2\, K_{on}}\;(v^\infty - v) \\ s_t \;+\; \dfrac{V_s}{V_v}\, s_x \;= j \\ j \;= \tilde{J}/K_{on} = \dfrac{Jh}{C_{s,max}\, K_{on}} = v\,(1-s) \;-\; \dfrac{K_{off}}{K_{on}}\; s \end{cases}$$

The dimensionless physical parameters appear directly in the above expression and we identify them:

$$\begin{aligned} d \;&=\; \frac{D}{l_D^2\, K_{on}} \\ \epsilon \;&=\; \frac{V_s}{V_v} \\ \alpha \;&=\; \frac{K_{off}}{K_{on}} \end{aligned}$$

This leads to the following system:

$$\begin{cases} v_t + v_x \;= -j \;+\; d(v^\infty - v) \\ s_t + \epsilon s_x \;= j \\ j = v\,(1-s) \;-\; \alpha s \end{cases} \tag{8}$$

[1] C. V. Denis, Molecular and Cellular Biology of von Willebrand Factor, International Journal of Hematology 75 (1) (2002) 3–8, ISSN 0925-5710.

[2] S. W. Schneider, S. Nuschele, A. Wixforth, C. Gorzelanny, A. Alexander-Katz, R. R. Netz, M. F. Schneider, Shear-induced unfolding triggers adhesion of von Willebrand factor fibers, Proceedings of the National Academy of Sciences 104 (19) (2007) 7899–7903.

[3] B. Fuchs, U. Budde, A. Schulz, C. M. Kessler, C. Fisseau, C. Kannicht, Flow-based measurements of von Willebrand factor (VWF) function: Binding to collagen and platelet adhesion under physiological shear rate, Thrombosis Research 125 (3) (2010) 239–245.

[4] M. Dembo, D. C. Torney, K. Saxman, D. Hammer, The Reaction-Limited Kinetics of Membrane-to-Surface Adhesion and Detachment, Proceedings of the Royal Society of London. Series B, Biological Sciences 234 (1274) (1988) pp. 55–83, ISSN 00804649.

[5] T. A. Doggett, G. Girdhar, A. Lawshé, D. W. Schmidtke, I. J. Laurenzi, S. L. Diamond, T. G. Diacovo, Selectin-Like Kinetics and Biomechanics Promote Rapid Platelet Adhesion in Flow: The GPIbα-vWF Tether Bond, Biophysical Journal 83 (1) (2002) 194 – 205, ISSN 0006-3495.

[6] S. P. Jackson, The growing complexity of platelet aggregation, Blood 109 (2007) 5087–5095.

[7] R. A. Kumar, J.-F. Dong, J. A. Thaggard, M. Cruz, J. A. Lopez, L. V. McIntire, Kinetics of GPIbα-vWF-A1 Tether Bond under Flow: Effect of GPIbα Mutations on the Association and Dissociation Rates, Biophysical Journal 85 (6) (2003) 4099 – 4109, ISSN 0006-3495.

[8] C. Dong, X. X. Lei, Biomechanics of cell rolling: shear flow, cell-surface adhesion, and cell deformability, Journal of Biomechanics 33 (1) (2000) 35 – 43, ISSN 0021-9290.

[9] P.-L. Tremblay, J. Huot, F. A. Auger, Mechanisms by which E-Selectin Regulates Diapedesis of Colon Cancer Cells under Flow Conditions, Cancer Research 68 (13) (2008) 5167–5176.

[10] T.Yago, J. Lou, T. Wu, J. Yang, J. J. Miner, L. Coburn, J. A. López, M. A. Cruz, J.-F. Dong, L. V. McIntire, R. P. McEver, C. Zhu, Platelet glycoprotein Ibα forms catch bonds with human WT vWF but not with type 2B von Willebrand disease vWF, The Journal of Clinical Investigation 118 (9) (2008) 3195–3207.

[11] M. Toner, D. Irimia, BLOOD-ON-A-CHIP, Annual Review of Biomedical Engineering 7 (1) (2005) 77–103.

[12] T. V. Colace, G. W. Tormoen, O. J. T. McCarty, S. L. Diamond, Microfluidics and Coagulation Biology, Annual Review of Biomedical Engineering 15 (2013) 283–303.

[13] S. F. Maloney, L. F. Brass, S. L. Diamond, P2Y12 or P2Y1inhibitors reduce platelet deposition in a microfluidic model of thrombosis while apyrase lacks efficacy under flow conditions, Integr. Biol. 2 (2010) 183–192.

[14] B. Lincoln, A. J. Ricco, N. J. Kent, L. Basabe-Desmonts, L. P. Lee, B. D. MacCraith, D. Kenny, G. Meade, Integrated system investigating shear-mediated platelet interactions with von Willebrand factor using microliters of whole blood, Analytical Biochemistry 405 (2) (2010) 174–183.

[15] K. S. Sakariassen, H. R. Baumgartner, Axial Dependence of Platelet-Collagen Interactions in Flowing Blood, ATVB 9 (1989) 33–42.

[16] E. Eckstein, F. Belgacem, Model of platelet transport in flowing blood with drift and diffusion terms, Biophysical Journal 60 (1) (1991) 53 – 69, ISSN 0006-3495.

[17] H. Zhao, E. S. G. Shaqfeh, V. Narsimhan, Shear-induced particle migration and margination in a cellular suspension, Physics of Fluids 24 (1) 011902.

[18] M. Lopez, M. D. Graham, Shear-induced diffusion in dilute suspensions of spherical or nonspherical particles: Effects of irreversibility and symmetry breaking, Physics of Fluids 19 (7) 073602.

[19] G. M. Whitesides, E. Ostuni, S. Takayama, X. Jiang, D. E. Ingber, SOFT LITHOGRAPHY IN BIOLOGY AND BIOCHEMISTRY, Annual Review of Biomedical Engineering 3 (1) (2001) 335–373.

[20] C. Dunois-Lardé, C. Capron, S. Fichelson, T. Bauer, E. Cramer-Bordé, D. Baruch, Exposure of human megakaryocytes to high shear rates accelerates platelet production, Blood 114 (9) (2009) 1875–1883.

[21] L. E. Corum, V. Hlady, The effect of upstream platelet–fibrinogen interactions on downstream adhesion and activation, Biomaterials 33 (2012) 1255–1260.

[22] M. M. Frojmovic, J. G. Milton, Human platelet size, shape and related functions in health and disease, Physiological Review 62 (1982) 185–261.

[23] S. Fitzgibbon, J. Cowman, A. J. Ricco, D. Kenny, E. S. G. Shaqfeh, Examining platelet adhesion via Stokes flow simulations and microfluidic experiments, Soft Matter 11 (2015) 355–367.

[24] K. Leiderman, A. L. Fogelson, Grow with the flow: a spatial–temporal model of platelet deposition and blood coagulation under flow, Mathematical Medicine and Biology 28 (1) (2011) 47–84.

[25] J. O. Taylor, L. Yang, S. Deutsch, K. B. Manning, Development of a platelet adhesion transport equation for a computational thrombosis model, Journal of Biomechanics 50 (2017) 114–120, URL `http://dx.doi.org/10.1016/j.jbiomech.2016.11.012`.

[26] R. Rusconi, H. A. Stone, Shear-Induced Diffusion of Platelike Particles in Microchannels, Physical Review Letters 101 (2008) 254502.

[27] T. M. Squires, R. J. Messinger, S. R. Manalis, Making it stick: convection, reaction and diffusion in surface-based biosensors, Nature Biotechnology 26 (2008) 417–426.

[28] M. E. Combariza, X. Yu, W. S. Nesbitt, A. Mitchell, F. J. Tovar-Lopez, Nonlinear Dynamic Modelling of Platelet Aggregation via Microfluidic Devices, IEEE transactions on biomedical engineering 62 (2015) 1718–1727.

[29] S. Rugonyi, Effect of Blood Flow on Near-the-Wall Mass Transport of Drugs and Other Bioactive Agents: A Simple Formula to Estimate Boundary Layer Concentrations, Journal of Biomechanical Engineering 130 (2008) 021010.

Exp	H (μm)	PLT source batch number	$[PLT]$ (mL^{-1})	$\dot{\gamma}$ (s^{-1})
A	23	1	$1.4{\cdot}10^8$	1400
B	23	2	$2.8{\cdot}10^8$	1800
C	63	3	$1.4{\cdot}10^8$	1800

Table 3: Conditions corresponding to the experimental results. Three different batches of platelets were tested. We varied channel height H, platelet concentration in the suspension $[PLT]$ as well as wall shear rate $\dot{\gamma}$. Sample A corresponds to data shown in Figures 9 to 13, samples B and C to data shown in Figure 14.

Supplementary Material

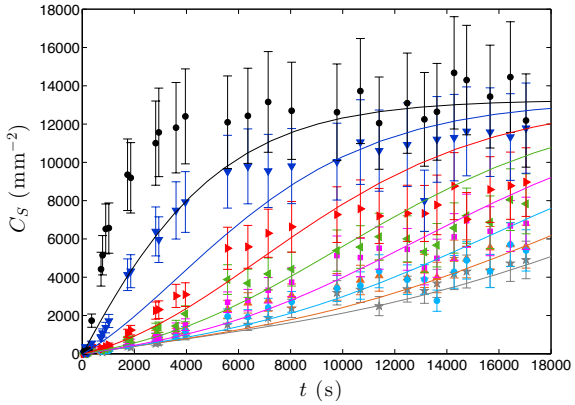

Figure 12: Temporal evolution of platelet surface concentration at different positions in the channel: $x = 0.6$ mm (●) $x = 1.6$ mm (▼), $x = 2.6$ mm (▶), $x = 3.6$ mm (◀), $x = 4.6$ mm (■), $x = 5.6$ mm (●), $x = 6.6$ mm (▲), $x = 7.6$ mm ($\star$). The experimental points with their error bar are compared with the model obtained when no rolling is considered (lines).

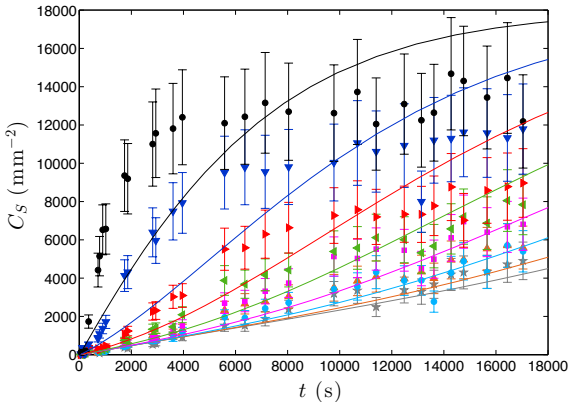

Figure 13: Temporal evolution of platelet surface concentration at different positions in the channel: $x = 0.6$ mm (●) $x = 1.6$ mm (▼), $x = 2.6$ mm (▶), $x = 3.6$ mm (◀), $x = 4.6$ mm (■), $x = 5.6$ mm (●), $x = 6.6$ mm (▲), $x = 7.6$ mm (⋆). The experimental points with their error bar are compared with the linear model (lines).

Exp	$C_{s,max}$ (mm^{-2})	V_v (mm·s^{-1})	K_{on} (s^{-1})	K_{off} (s^{-1})	D (mm^{2}s^{-1})	h (mm)
B	$3.8 \cdot 10^4$	0.01	$7.2 \cdot 10^{-3}$	$1.4 \cdot 10^{-4}$	$1.8 \cdot 10^{-10}$	$1.1 \cdot 10^{-3}$
C	$6.8 \cdot 10^4$	0.12	0.16	$8.0 \cdot 10^{-4}$	$2.5 \cdot 10^{-6}$	$4.9 \cdot 10^{-4}$

Table 4: Parameters obtained by fitting data shown in Figure 14 with a model neglecting rolling.

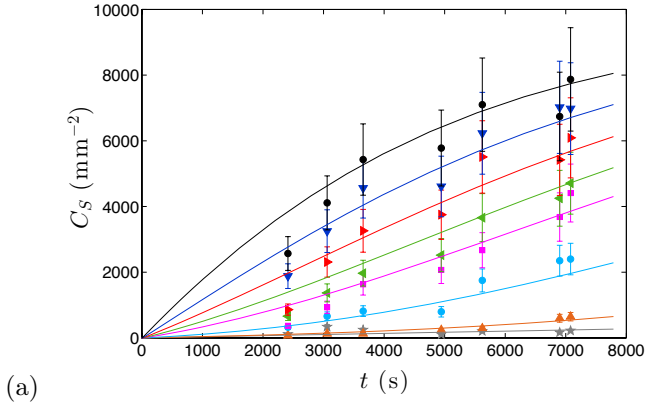

(a)

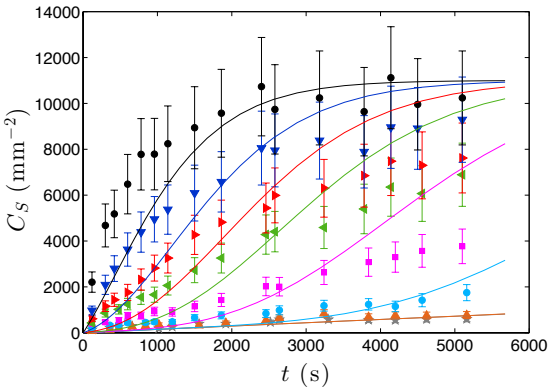

(b)

Figure 14: Adjustments of two extra experimental kinetics with the model neglecting rolling. The experimental parameters are listed in Table 3. (a) Curves obtained for sample B at positions $x = 0.5$ mm (●) $x = 1$ mm (▼), $x = 1.5$ mm (▶), $x = 2$ mm (◀), $x = 2.5$ mm (■), $x = 4$ mm (●), $x = 7$ mm (▲), $x = 38$ mm (⋆). (b) Curves obtained for sample C at positions $x = 0.5$ mm (●) $x = 1$ mm (▼), $x = 1.5$ mm (▶), $x = 2$ mm (◀), $x = 3$ mm (■), $x = 5$ mm (●), $x = 10$ mm (▲), $x = 30$ mm (⋆).